Supporting Information
Prospect of high-temperature superconductivity in layered metal borocarbides

Charlsey R. Tomassetti,[1] Gyanu P. Kafle,[1] Edan T. Marcial,[1] Elena R. Margine,[1,*] and Aleksey N. Kolmogorov[1,†]

[1] *Department of Physics, Applied Physics, and Astronomy, Binghamton University-SUNY, Binghamton, New York 13902, USA*

(Dated: February 29, 2024)

I Supplementary Figure S1 Comparison of reported and simulated power XRD patterns for Li_xBC 2

II Supplementary Figures S2-S4 Electronic, vibrational, and superconducting properties of Li_xBC with $\frac{5}{6} \geq x \geq \frac{1}{2}$ ... 3-5

III Supplementary Figures S5-S7 Electronic, vibrational, and superconducting properties of $Li_{1/2}BC$ with distortions . 6-8

IV Supplementary Figures S8-S9 Electronic, vibrational, and e-ph coupling properties of $Li_{1/2}BC$ with defects 9-10

V Supplementary Figure S10 Relative stability of Li_xM_yBC phases for $x = \frac{3}{4}, \frac{2}{3}, \frac{5}{8}, \frac{1}{2}$ and M = Na, K, Mg, and Ca ... 11

VI Supplementary Figure S11 Stability of $M_{1/2}BC$ and Li_xM_yBC phases with defects for M = Na, K, Mg, and Ca ... 12

VII Supplementary Figure S12 Global stability of layered Li_xM_yBC phases for M = Na, K, Mg, and Ca at $T = 0$ K.... 13

VIII Supplementary Figure S13 Projected phonon DOS in NaBC and $Li_{1/2}Na_yBC$ 14

IX Supplementary Figure S14 Global stability of predicted NaBC and $Li_{1/2}Na_yBC$ calculated with optB88-vdW 15

X Supplementary Figure S15 Quasi-harmonic energy corrections 16

XI Supplementary Figure S16 Quasi-harmonic energy correction to global stability of NaBC and $Li_{1/2}Na_{1/2}BC$ 17

XII Supplementary Figures S17-S21 Electronic, vibrational, and superconducting properties of Li_xM_yBC phases 17-21

XIII Supplementary Figure S22 Accuracy of Wannier interpolated bands 22

XIV Supplementary Figure S23 Electronic, vibrational and superconducting properties of MgB_2 22

XV Supplementary Table S1 Structural information for select Li_xBC and Li_xM_yBC phases 23

XVI Supplementary Table S2 Computational settings in superconductivity calculations 24

* rmargine@binghamton.edu
† kolmogorov@binghamton.edu

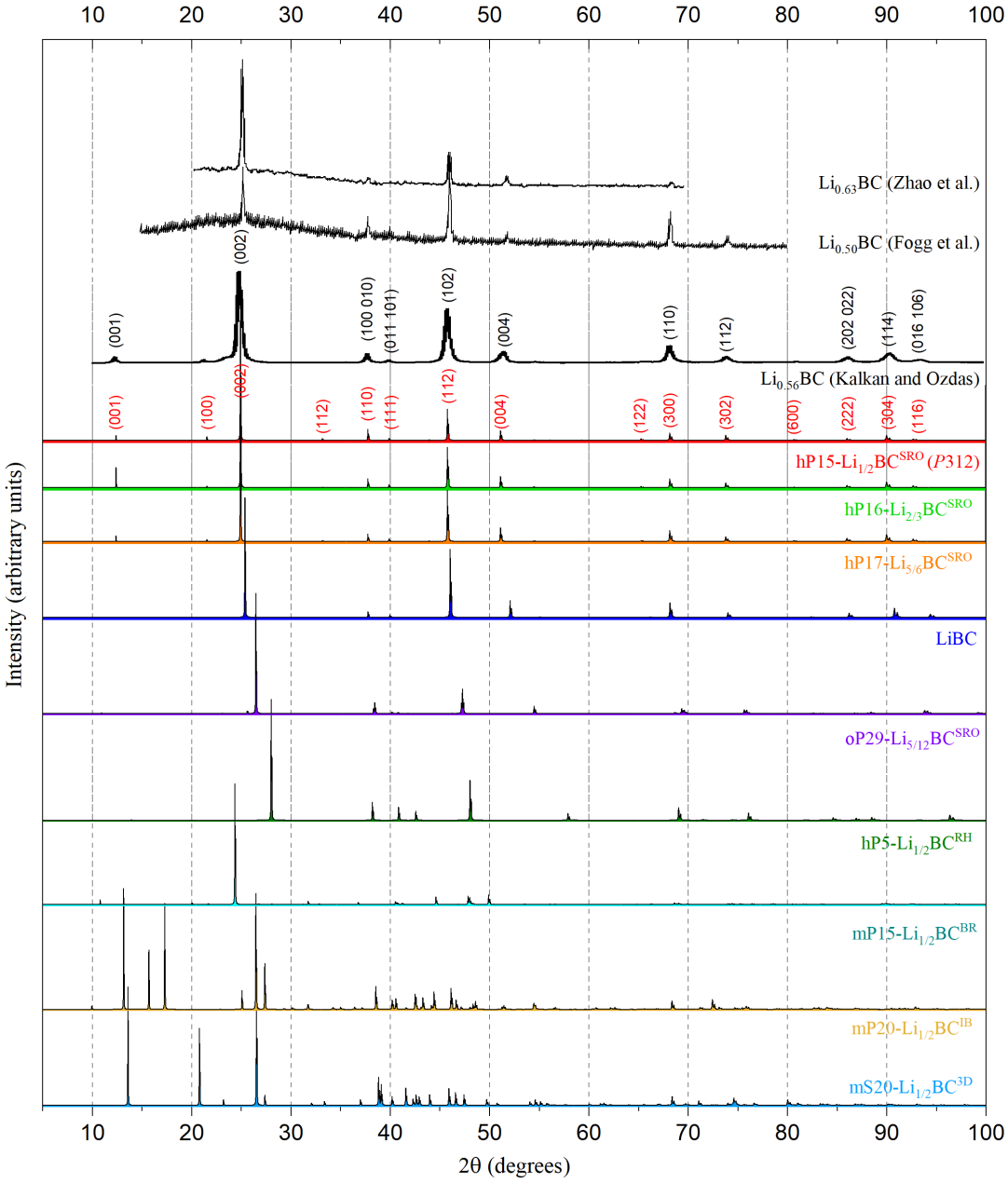

FIG. S1. Comparison of powder x-ray diffraction patterns obtained for synthesized Li_xBC samples (the top three data sets adopted from Refs. [1–3]) and simulated with $\lambda_{Cu\ K-\alpha} = 1.54059$ Å for Li_xBC models considered in this study (the bottom nine data sets).

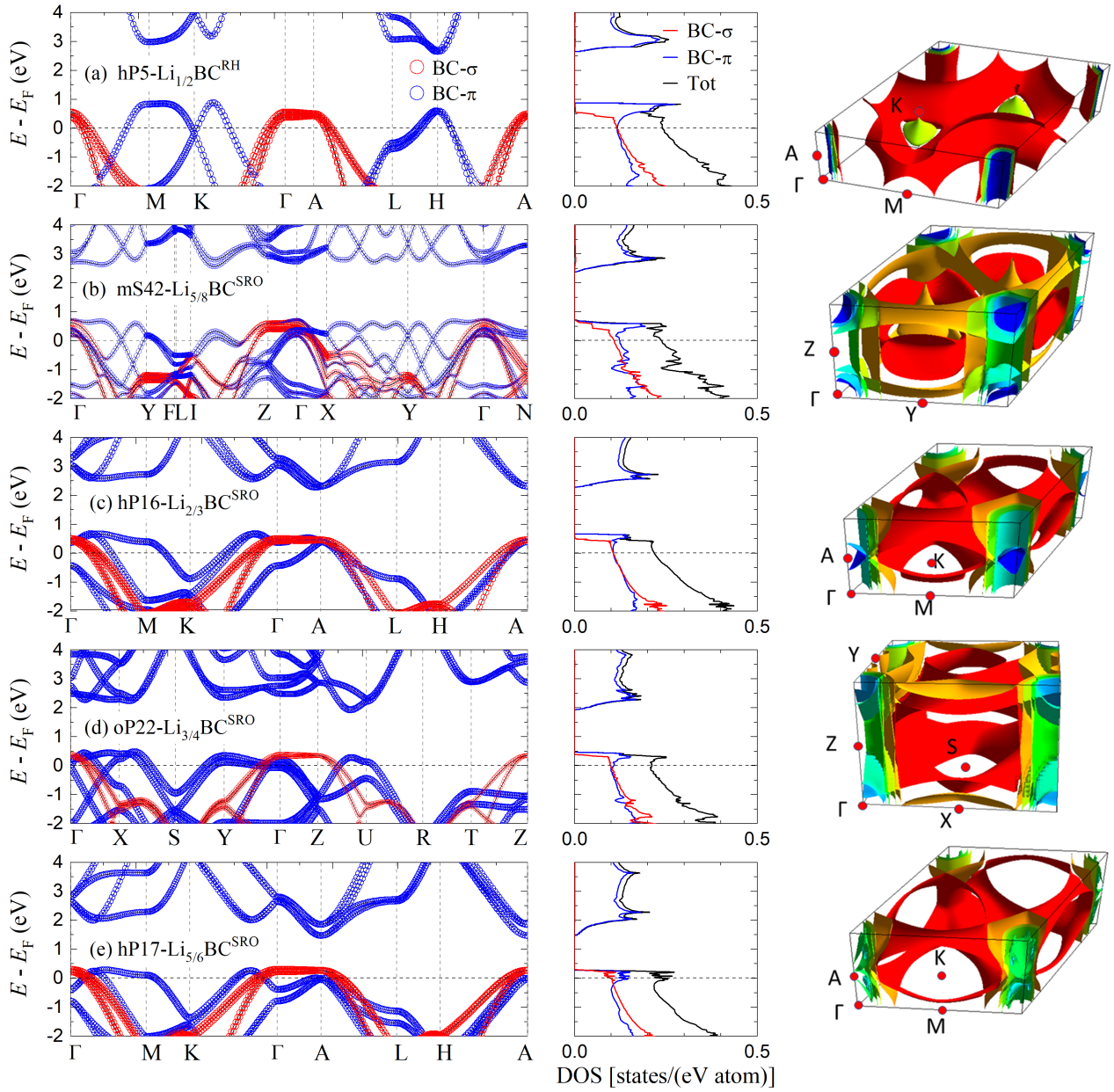

FIG. S2. Electronic properties of the five short-range ordering (SRO) or stage-2 configurations identified across the Li_xBC ($5/6 \geq x \geq 1/2$) compositions: (a) hP5-$Li_{1/2}BC^{RH}$, (b) mS42-$Li_{5/8}BC^{SRO}$, (c) hP16-$Li_{2/3}BC^{SRO}$, (d) oP22-$Li_{3/4}BC^{SRO}$, and (e) hP17-$Li_{5/6}BC^{SRO}$. Each row contains the electronic band structure with orbital characters (left panel), the total and projected DOS (middle panel), and the Fermi surfaces (right panel).

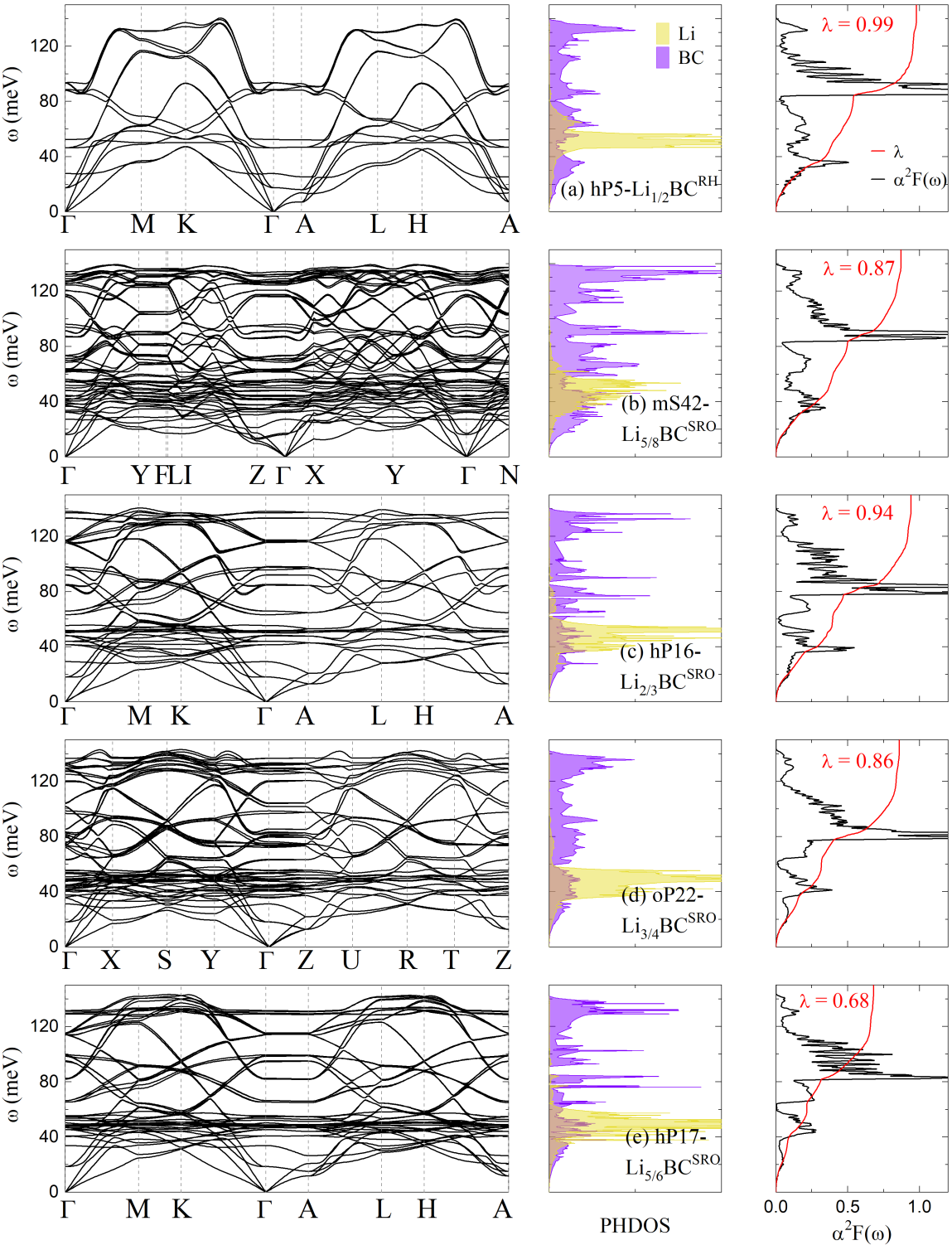

FIG. S3. Vibrational and e-ph coupling properties of the five short-range ordering (SRO) or stage-2 configurations identified across the Li_xBC ($5/6 \geq x \geq 1/2$) compositions: (a) hP5-$Li_{1/2}BC^{RH}$, (b) mS42-$Li_{5/8}BC^{SRO}$, (c) hP16-$Li_{2/3}BC^{SRO}$, (d) oP22-$Li_{3/4}BC^{SRO}$, and (e) hP17-$Li_{5/6}BC^{SRO}$. Each row contains the phononic dispersion (left panel), the phononic DOS decomposed into Li and BC contributions (middle panel), and the Eliashberg spectral function $\alpha^2F(\omega)$ with integrated e-ph coupling strength λ (right panel).

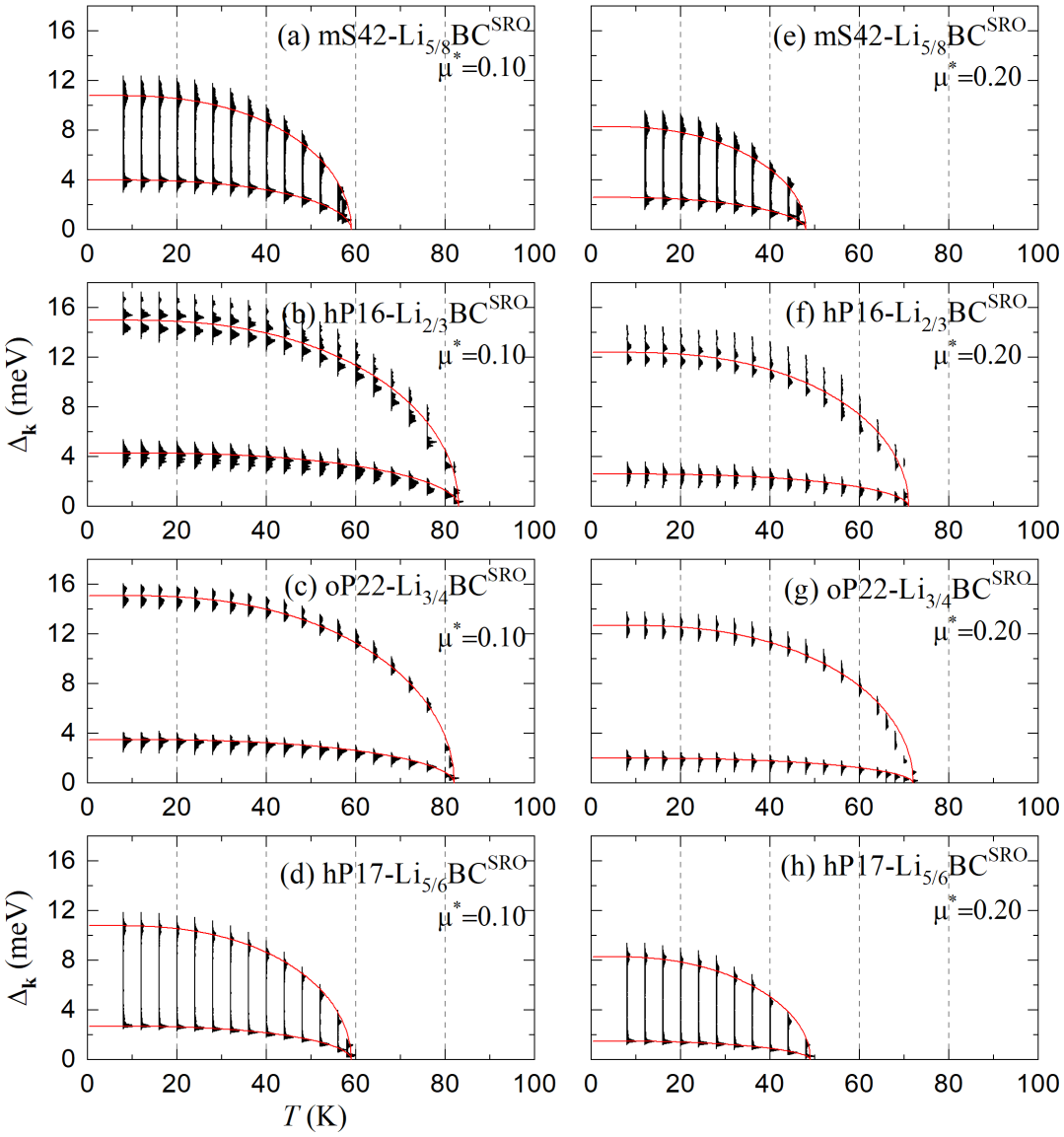

FIG. S4. Energy distribution of the superconducting gaps $\Delta_{\mathbf{k}}$ as a function of temperature with $\mu^* = 0.10$ and $\mu^* = 0.20$ for four short-range ordering (SRO) configurations identified across the Li_xBC ($5/6 \geq x \geq 5/8$) compositions: (a,e) mS42-$Li_{5/8}BC^{SRO}$, (b,f) hP16-$Li_{2/3}BC^{SRO}$, (c,g) oP22-$Li_{3/4}BC^{SRO}$, and (d,h) hP17-$Li_{5/6}BC^{SRO}$. The red curves are a guide for the eye.

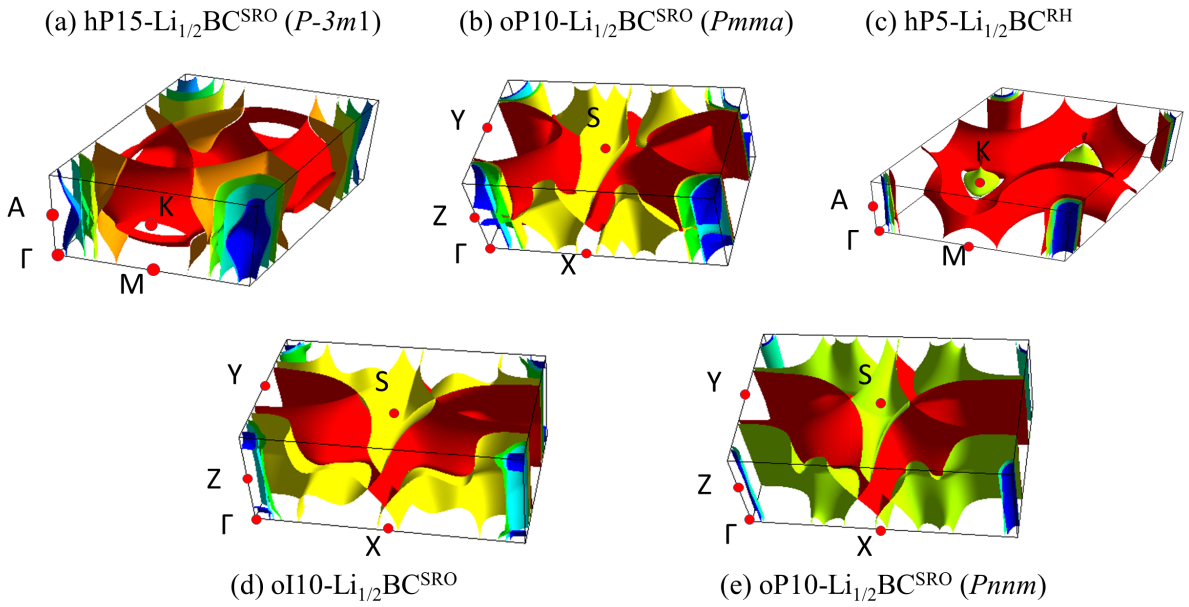

FIG. S5. Fermi surfaces for $Li_{1/2}BC$ layered configurations (a) hP15^{SRO} ($P\bar{3}m1$), (b) oP10^{SRO} ($Pmma$), (c) hP5^{RH}, (d) oI10^{SRO}, and (e) oP10^{SRO} ($Pnnm$), with the degree of BC layer distortion increasing from (a) to (e).

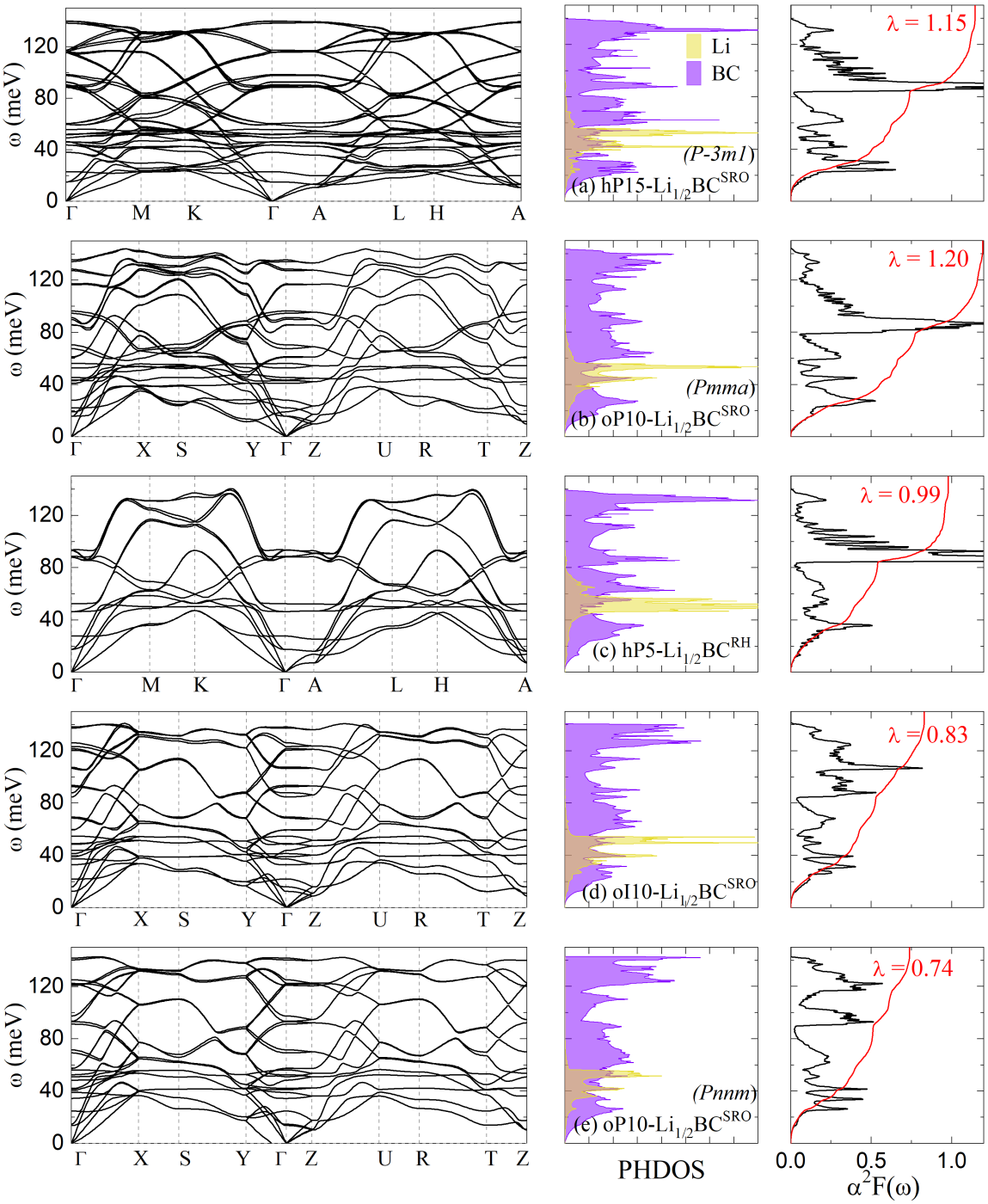

FIG. S6. Vibrational and e-ph coupling properties in $Li_{1/2}BC$ layered configurations (a) hP15^{SRO} ($P\bar{3}m1$), (b) oP10^{SRO} ($Pmma$), (c) hP5^{RH}, (d) oI10^{SRO}, and (e) oP10^{SRO} ($Pnnm$), with the degree of BC layer distortion increasing from (a) to (e). Each row contains the phononic dispersion (left panel), the phononic DOS decomposed into Li and BC contributions (middle panel), and the Eliashberg spectral function $\alpha^2F(\omega)$ with integrated e-ph coupling strength λ (right panel).

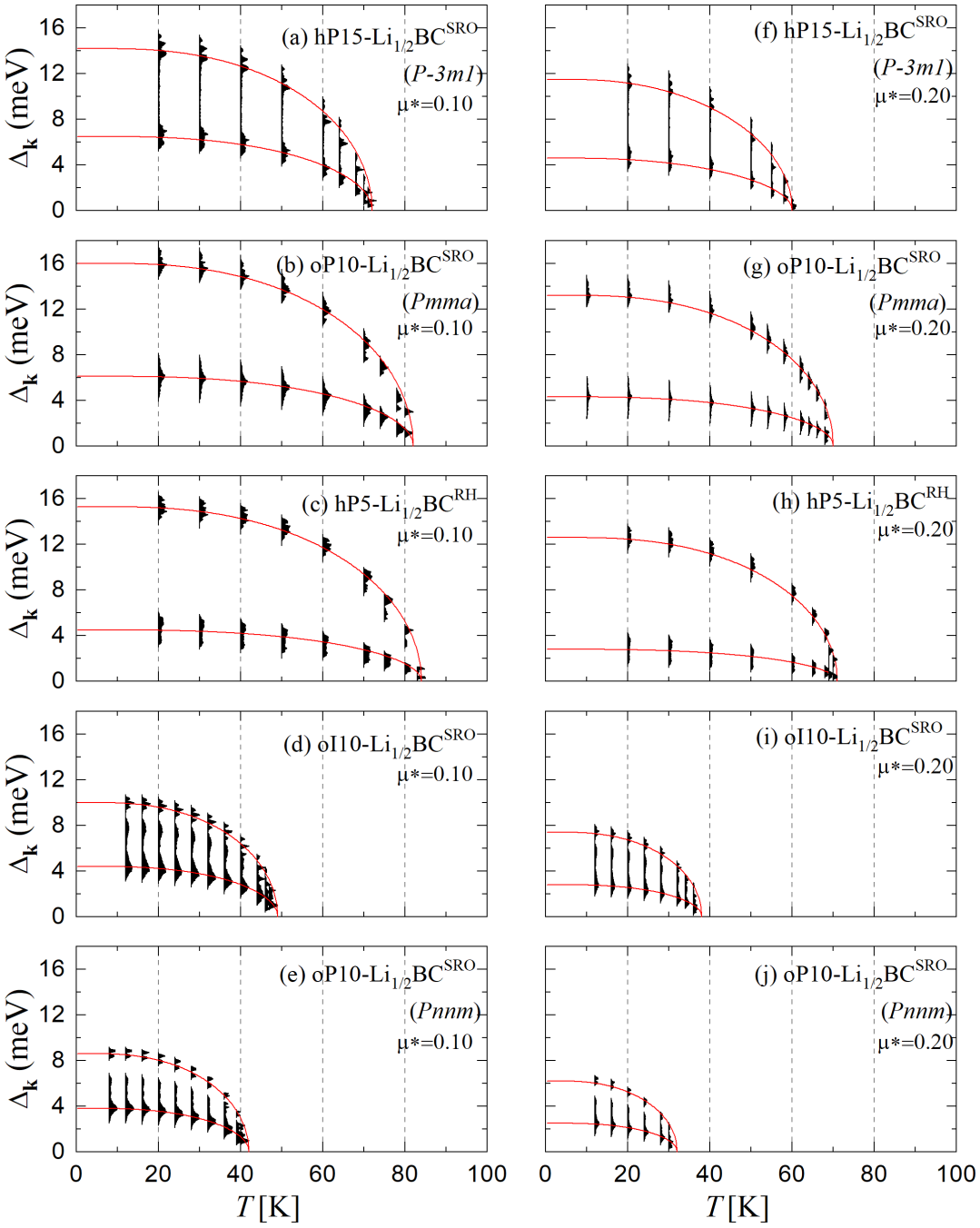

FIG. S7. Energy distribution of the superconducting gaps $\Delta_{\mathbf{k}}$ as a function of temperature with $\mu^* = 0.10$ (left panels) and $\mu^* = 0.20$ (right panels) for $Li_{1/2}BC$ layered configurations (a, f) hP15^{SRO} ($P\bar{3}m1$), (b, g) oP10^{SRO} ($Pmma$), (c, h) hP5^{RH}, (d, i) oI10^{SRO}, and (e, j) oP10^{SRO} ($Pnnm$), arranged in increasing order of BC layer distortion. The red curves are a guide for the eye.

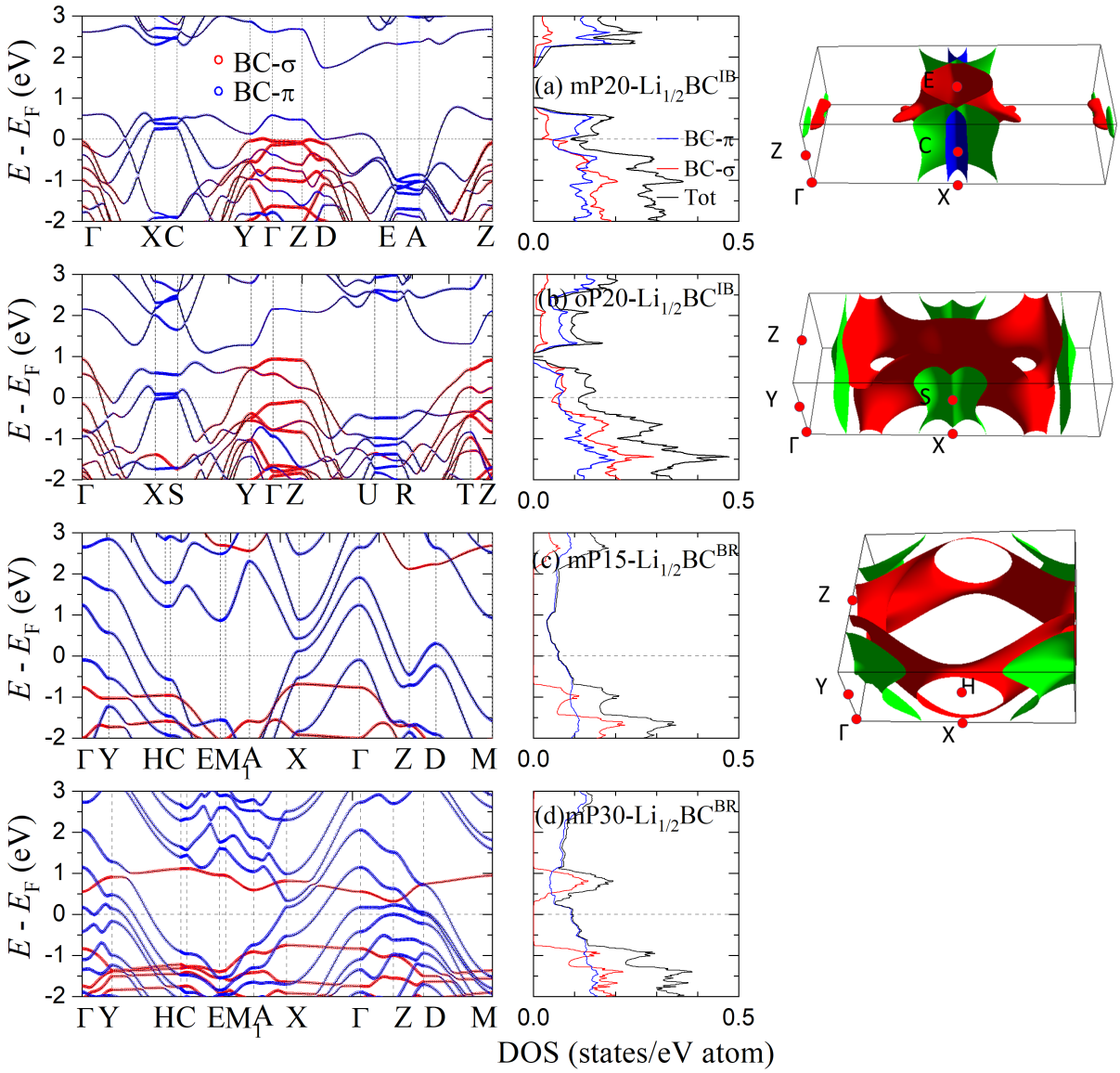

FIG. S8. Electronic properties for $Li_{1/2}BC$ layered configurations with interlayer bridging (IB) and bond rotation (BR) defects: (a) mP20-$Li_{1/2}BC^{IB}$, (b) oP20-$Li_{1/2}BC^{IB}$, (c) mP15-$Li_{1/2}BC^{BR}$, and (d) mP30-$Li_{1/2}BC^{BR}$. Each row contains the electronic band structure with orbital characters (left panel), the total and projected DOS (middle panel), and the Fermi surfaces (right panel).

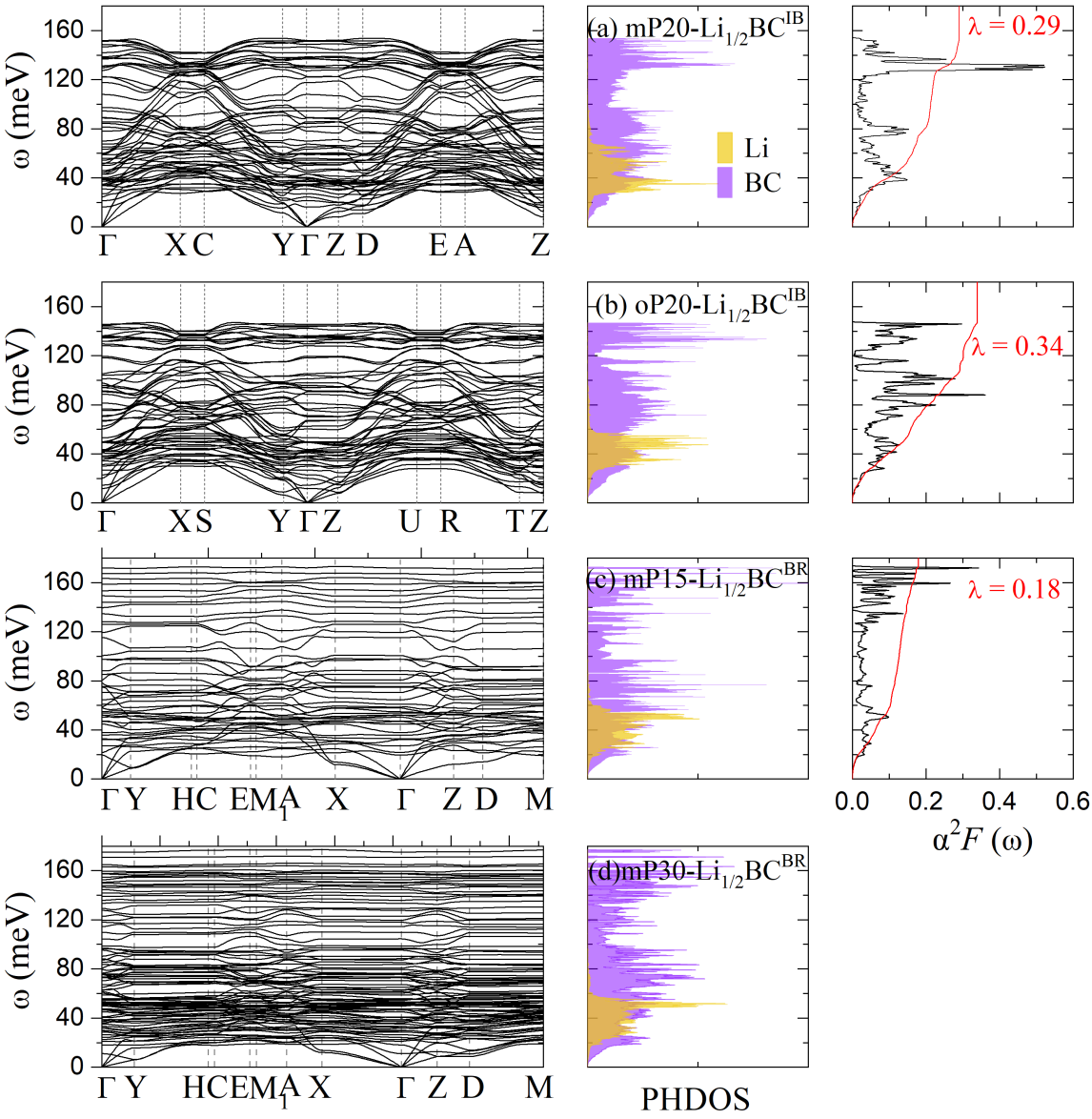

FIG. S9. Vibrational and e-ph coupling properties in $Li_{1/2}BC$ layered configurations with interlayer bridging (IB) and bond rotation (BR) defects: (a) mP20-$Li_{1/2}BC^{IB}$, (b) oP20-$Li_{1/2}BC^{IB}$, (c) mP15-$Li_{1/2}BC^{BR}$, and (d) mP30-$Li_{1/2}BC^{BR}$. Each row contains the phononic dispersion (left panel), the phononic DOS decomposed into Li and BC contributions (middle panel), and the Eliashberg spectral function $\alpha^2F(\omega)$ with integrated e-ph coupling strength λ (right panel).

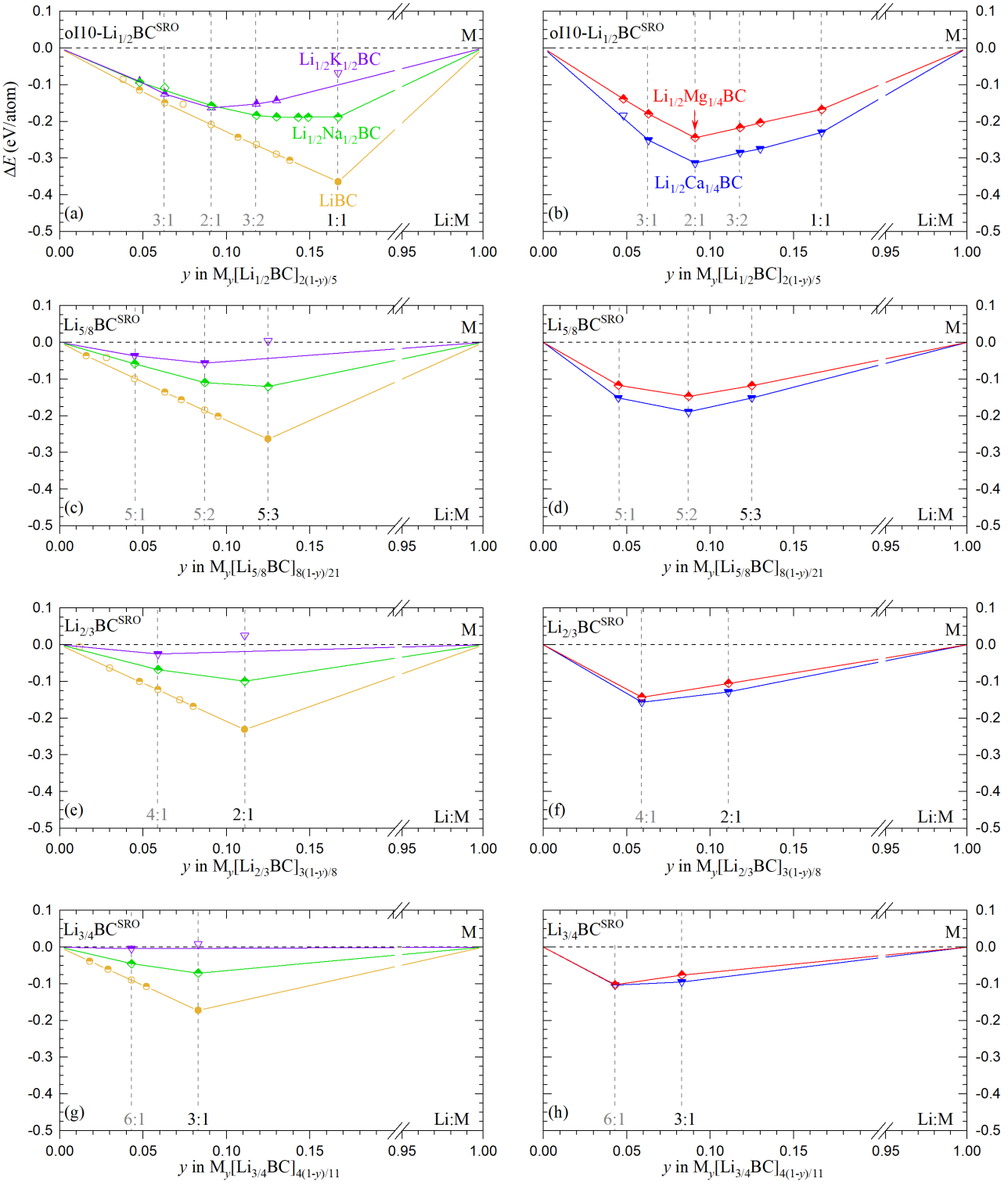

FIG. S10. Relative energies of $Li_xM_{[(x+2)y/(1-y)]}BC$ phases referenced to the lowest energy honeycomb layered phases Li_xBC ($3/4 \geq x \geq 1/2$) and pure M. The stable LiBC is marked with a solid circle. Metastable phases defining the local convex hull in the kinetically-protected subspace of layered borocarbides are shown as half-filled points connected with solid lines. The results indicate that it is thermodynamically favorable for the Na, K, Mg, and Ca metals to intercalate into the starting Li_xBC material for all considered *fixed* values of x. Information on the *global* stability of the Li_xM_yBC phases can be found in Figs. 8 and S12.

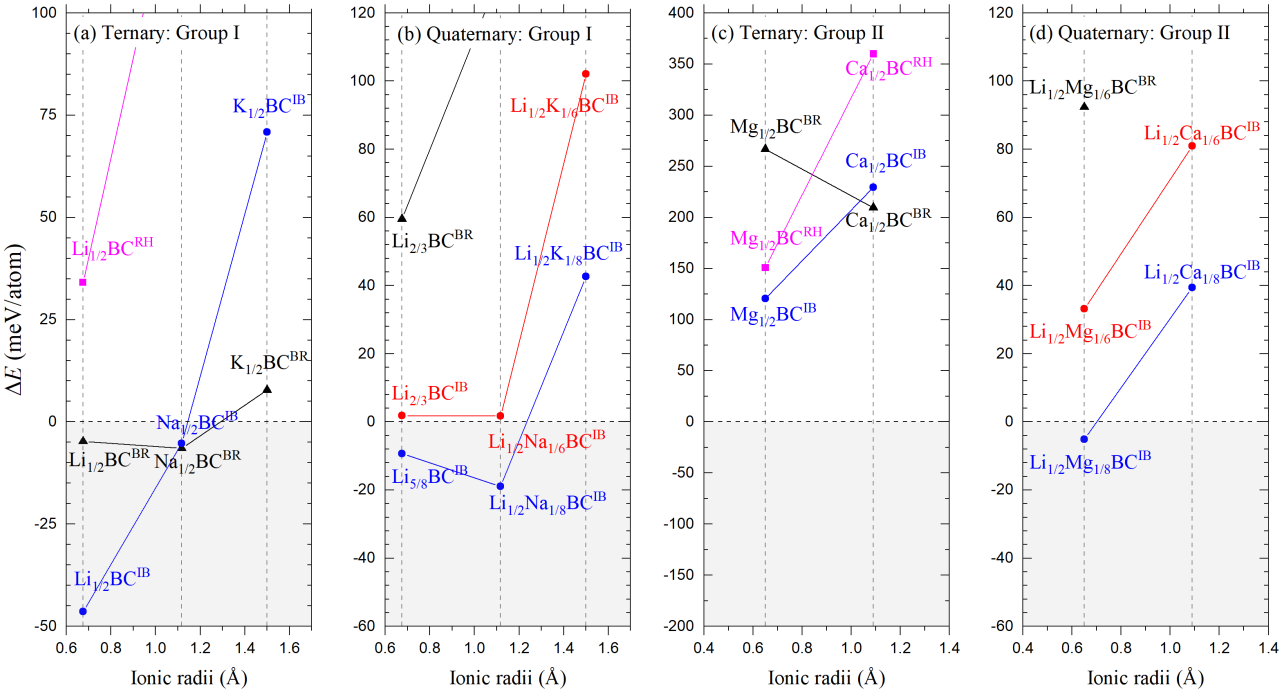

FIG. S11. Relative energies of (a,c) $M_{1/2}BC$ ternaries and (b,d) a selection of $Li_{1/2}M_yBC$ quaternaries with structural transformations referenced to their lowest energy ordered phase with a hexagonal BC network at that composition, plotted versus the ionic radius of the M intercalant [4]. The "BR" transformation refers to in-plane bond rotations resulting in a swap of B and C atoms. The "IB" transformation refers to interlayer bridging leading to the formation of C-C interlayer bonds. The "RH" refers to Rüdorff-Hofmann stage-2 configuration.

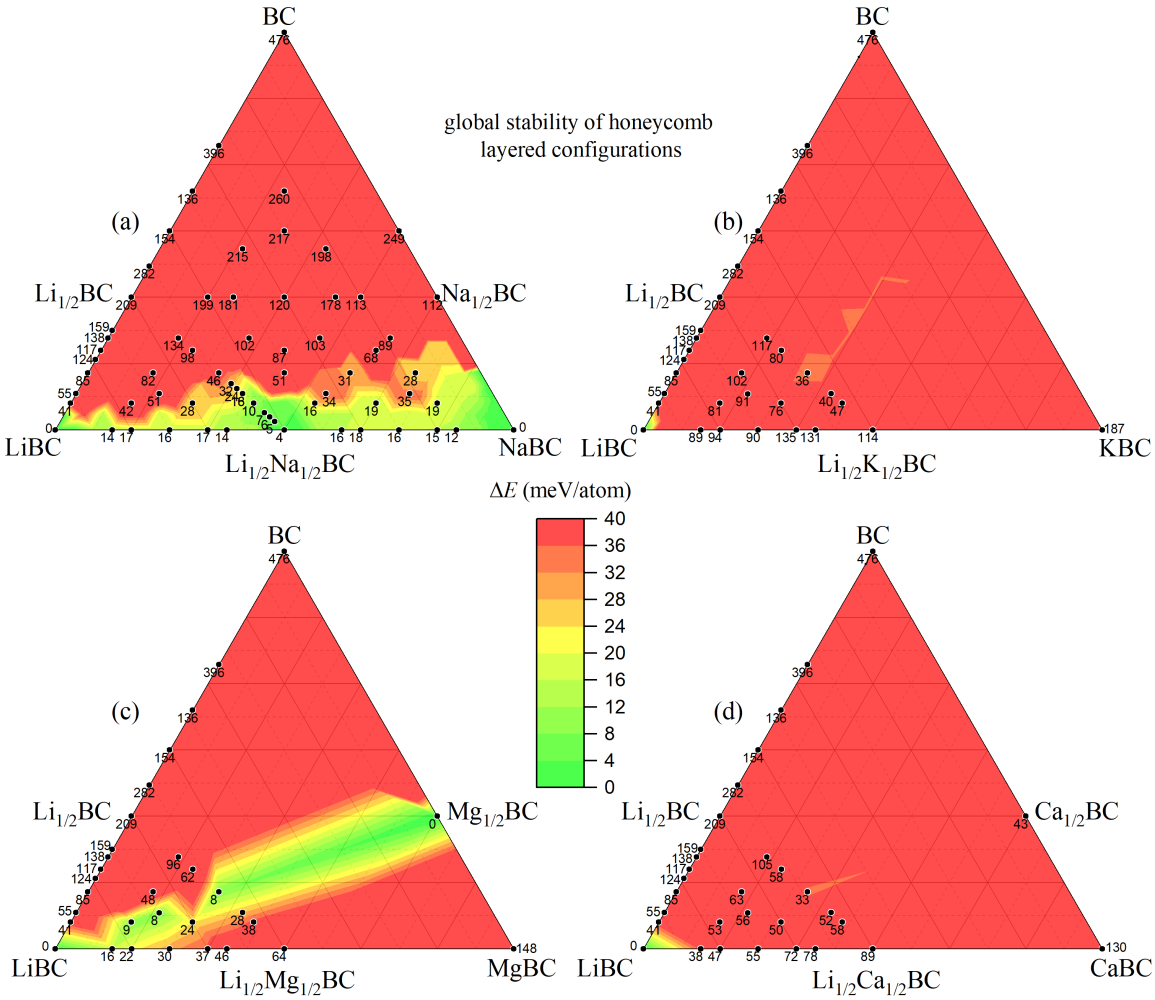

FIG. S12. Distance to the global convex hull for Li_xM_yBC phases with honeycomb morphology at $T = 0$ K. For the elemental metals, we considered cI2, cF4 and hP2 configurations and used the most stable representation with the optB86b functional. The convex hull for each quaternary was constructed using the full set of synthesized materials reported in the literature or proposed compounds discussed in our study: cF4-Li, hR36-B, hP4-C, cF4-Na, hP2-Mg, cF4-K, cF4-Ca, tP16-LiB_3, hP15-Li_8B_7, tP136-$Li_{24}B_{112}$, hP34-$Li_{18}B_{16}$, hP13-LiC_{12}, hP7-LiC_6, mS14-Li_8C_6, mS30-B_4C, oF46-Na_6B_{40}, oI64-Na_4B_{60}, hP6-NaBC, aP189-NaB_5C, oP14-NaB_5C, hP6-LiBC, oI64-$LiB_{13}C_2$, oF32-LiB_6C, oS80-MgB_2C_2, oI60-$MgB_{12}C_2$, tP54-$Mg_2B_{24}C$, hP3-MgB_2, oP20-MgB_4, cP7-KB_6, oF72-KC_8, tI20-CaB_2C_2, mS12-CaC_2, hR21-CaC_6, tP20-CaB_4, and cP7-CaB_6. The phases are described in Refs. [5–9] and specified in the provided CIF files.

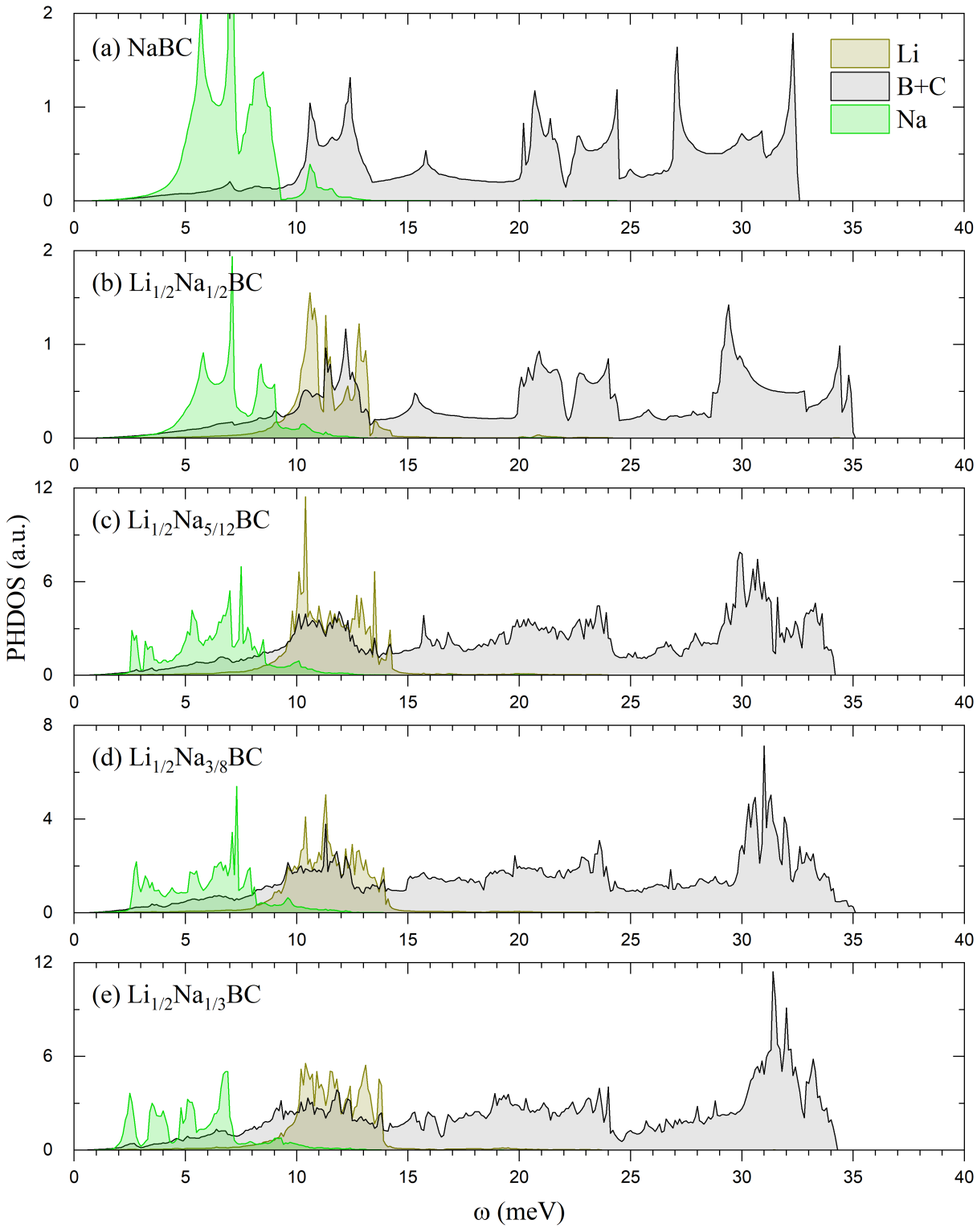

FIG. S13. Projected phononic DOS for NaBC and $Li_{1/2}Na_yBC$ calculated with the finite displacement method using PHONOPY and VASP. Details on the hP6-$Li_{1/2}Na_{1/2}BC$, mP35-$Li_{1/2}Na_{5/12}BC$, mP23-$Li_{1/2}Na_{3/8}BC$, and mP34-$Li_{1/2}Na_{1/3}BC$ phases can be found in main text Table 1. The removal of Na in the double-metal borocarbides, from $y = 1/2$ in (b) to $y = 1/3$ in (e), results in the softening of the Na modes.

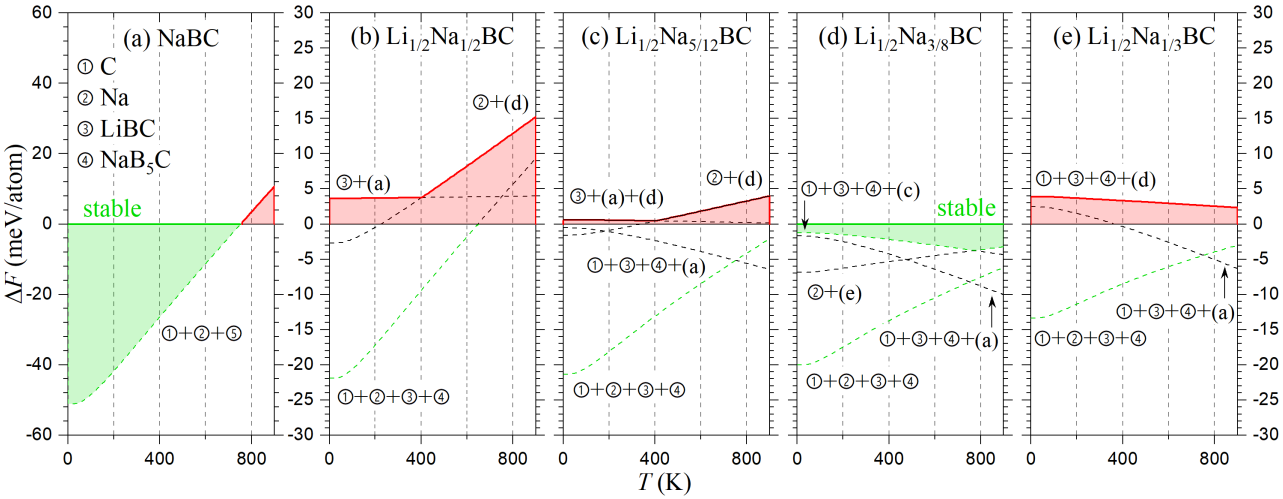

FIG. S14. Distance to the convex hull as a function of temperature for proposed Na and Li-Na borocarbides calculated with the optB88 functional [10]. Different lines correspond to the lowest-free energy combinations among all observed ground states (circled numbers) and proposed phases (bracketed letters). NaBC and $Li_{1/2}Na_yBC$ (y = 1/2, 5/12, and 3/8) appear thermodynamically stable at low temperatures with respect to any mixture of the synthesized Li-Na-B-C phases listed in Fig. S12. The displayed set of phases equals that in Figs. 8 and S13.

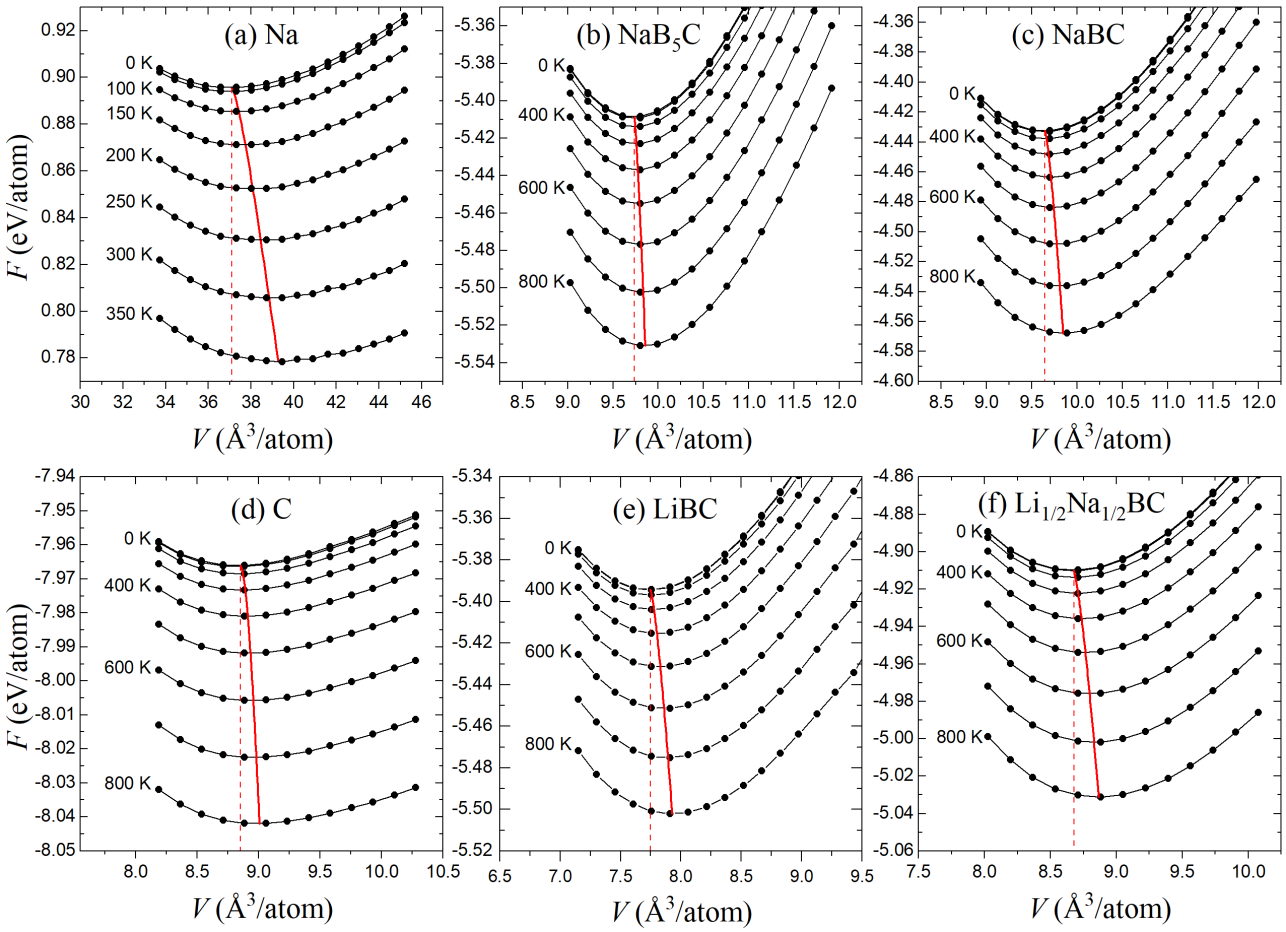

FIG. S15. Quasi-harmonic approximation (QHA) results for fcc-Na, oP14-NaB_5C, hP6-NaBC, hP4-C, hP6-LiBC and hP6-$Li_{1/2}Na_{1/2}BC$. In these simulations, we (i) generated a uniform grid of volumes around equilibrium by rescaling the lattice constants; (ii) optimized the unit cell shape and atomic positions at each fixed volume with VASP; (iii) used Phonopy and VASP to perform phonon calculations in the harmonic approximation at each volume; (iv) fitted the resulting free energy points at each temperature with a third-order polynomial; and (v) showed the free energy values for every (a) 50 K or (b-f) 100 K (black circles), the polynomial fits (black solid lines), the minimum free energy values at the corresponding volumes for every 10 K (red solid line), and the starting volume (red dashed line). At 800 K, the free energy difference between the standard harmonic formalism and the QHA values was found to be (b) -2.6 (c) -4.2 (d) -1.0 (e) -4.5 and (f) -4.4 meV/atom. At 350 K, the free energy difference for fcc-Na is -6.1 meV/atom.

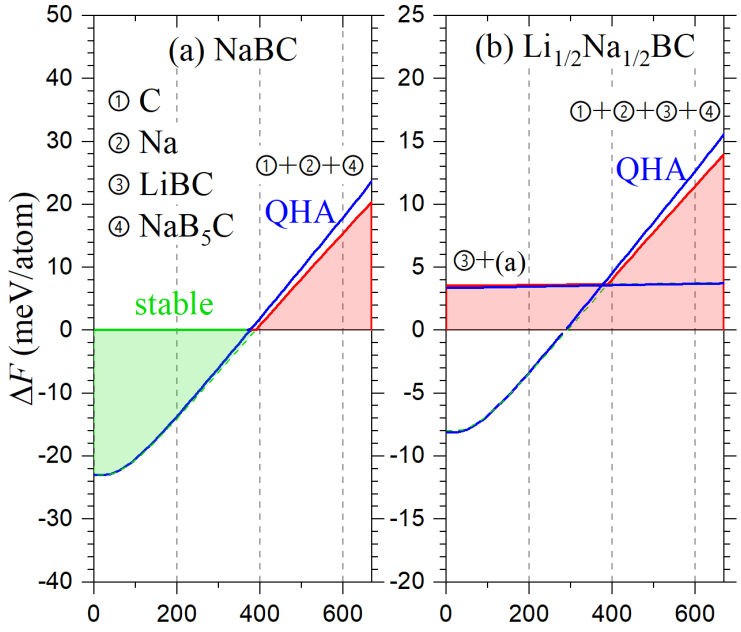

FIG. S16. Effect of the quasi-harmonic approximation (QHA) on the distance to the convex hull as a function of temperature for proposed NaBC and $Li_{1/2}Na_{1/2}BC$ calculated with the optB86b functional [11]. The distance to the convex hull using the QHA is shown as blue lines.

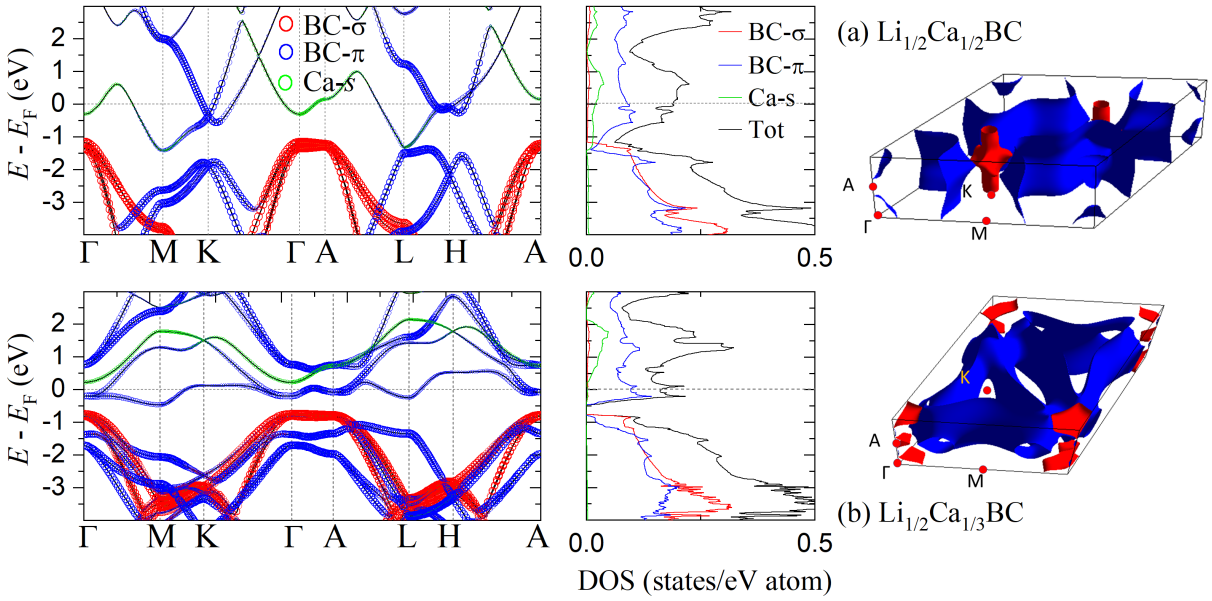

FIG. S17. Electronic properties for (a) $Li_{1/2}Ca_{1/2}BC$ and (b) $Li_{1/2}Ca_{1/3}BC$. Each row contains the electronic band structure with orbital characters (left panel), the total and projected DOS (middle panel), and the Fermi surfaces (right panel).

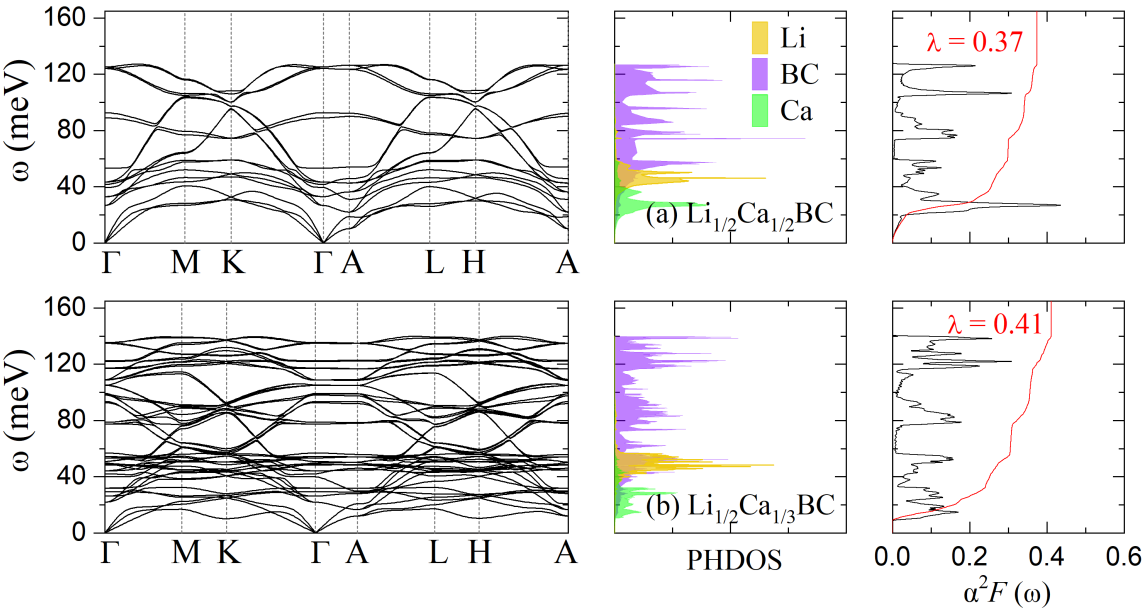

FIG. S18. Vibrational and e-ph coupling properties in (a) $Li_{1/2}Ca_{1/2}BC$ and (b) $Li_{1/2}Ca_{1/3}BC$. Each row contains the phononic dispersion (left panel), the phononic DOS decomposed into Li, Ca and BC contributions (middle panel), and the Eliashberg spectral function $\alpha^2F(\omega)$ with integrated e-ph coupling strength λ (right panel).

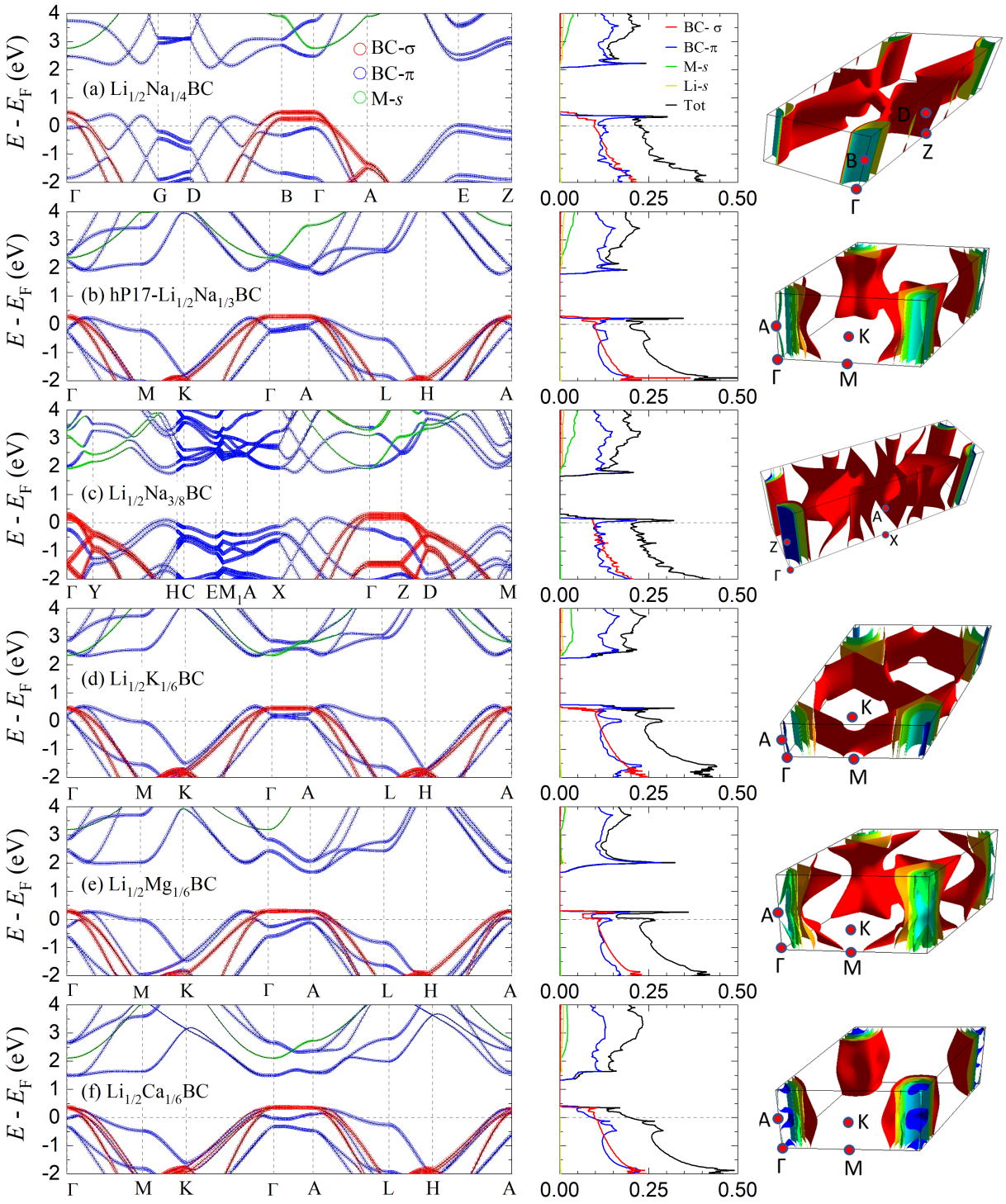

FIG. S19. Electronic properties for (a) $Li_{1/2}Na_{1/4}BC$, (b) hP17-$Li_{1/2}Na_{1/3}BC$, (c) $Li_{1/2}K_{1/6}BC$, (d) $Li_{1/2}Mg_{1/6}BC$, and (e) $Li_{1/2}Ca_{1/6}BC$. Each row contains the electronic band structure with orbital characters (left panel), the total and projected DOS (middle panel), and the Fermi surfaces (right panel).

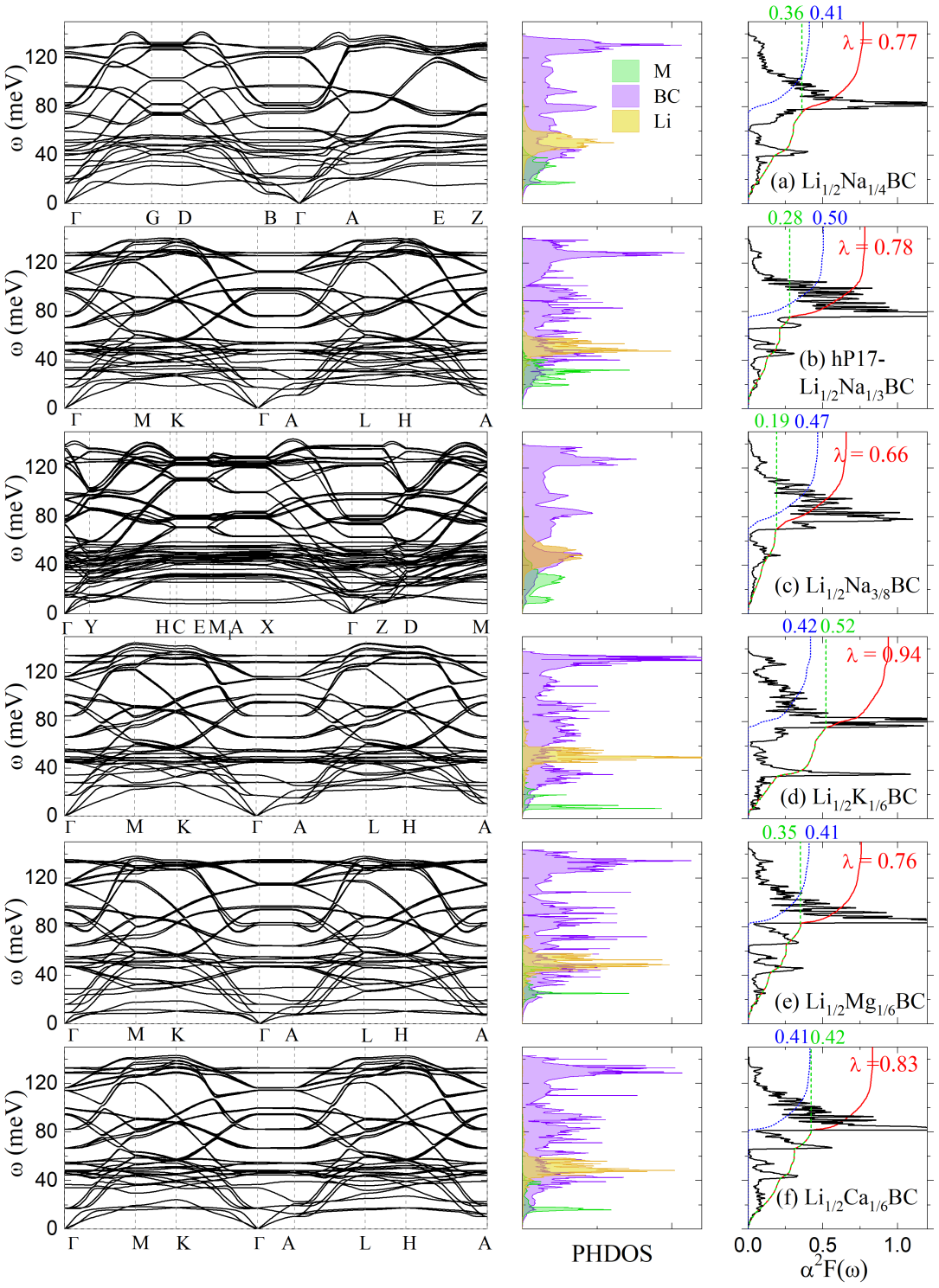

FIG. S20. Vibrational and e-ph coupling properties in (a) $Li_{1/2}Na_{1/4}BC$, (b) hP17-$Li_{1/2}Na_{1/3}BC$, (c) $Li_{1/2}K_{1/6}BC$, (d) $Li_{1/2}Mg_{1/6}BC$, and (e) $Li_{1/2}Ca_{1/6}BC$. Each row contains the phononic dispersion (left panel), the phononic DOS decomposed into Li, M and BC contributions (middle panel), and the Eliashberg spectral function $\alpha^2F(\omega)$ with integrated e-ph coupling strength λ (right panel). The partial e-ph coupling strength from modes above and below (a-b,d) 75, (c) 70, or (e-f) 80 meV are shown as the dotted blue and dashed green lines, respectively.

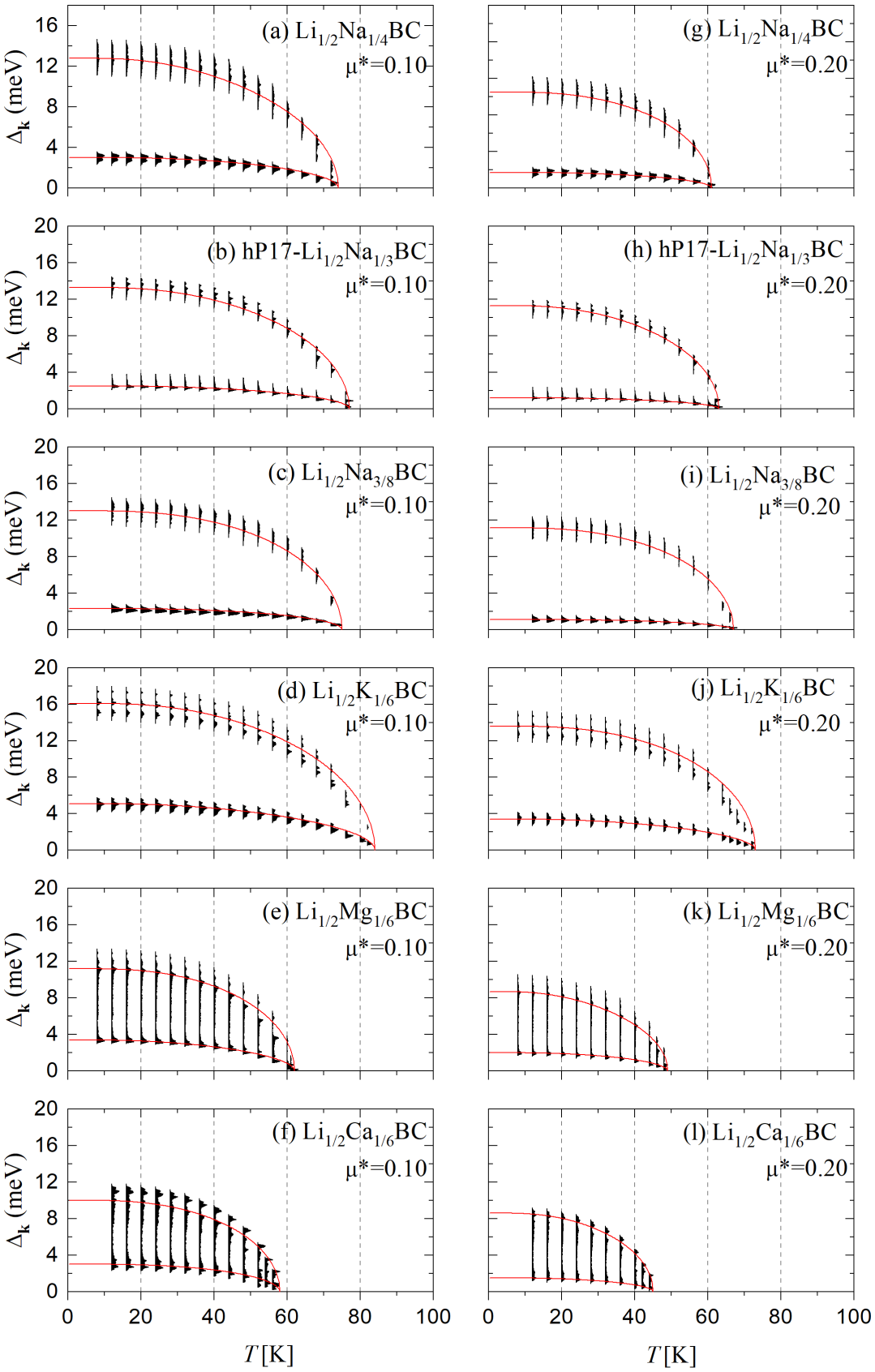

FIG. S21. Energy distribution of the superconducting gaps $\Delta_{\mathbf{k}}$ as a function of temperature with $\mu^* = 0.10$ (left panels) and $\mu^* = 0.20$ (right panels) for (a, g) $Li_{1/2}Na_{1/4}BC$, (b, h) hP17-$Li_{1/2}Na_{1/3}BC$, (c, i) $Li_{1/2}Na_{3/8}BC$ (d, j) $Li_{1/2}K_{1/6}BC$, (e, k) $Li_{1/2}Mg_{1/6}BC$, and (f, l) $Li_{1/2}Ca_{1/6}BC$. The red curves are a guide for the eye.

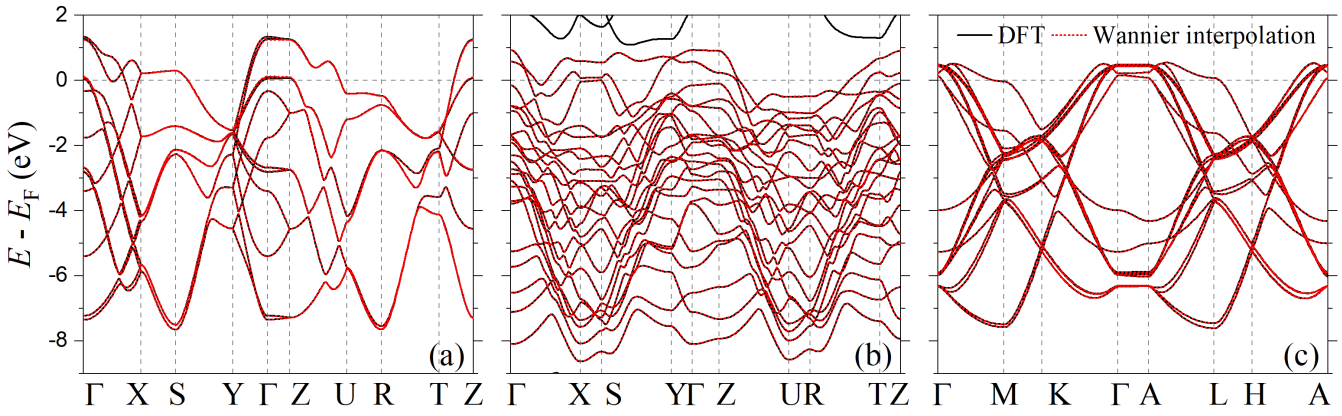

FIG. S22. Comparison of band structures obtained with DFT and Wannier interpolation for representative phases (a) oP10-$Li_{1/2}BC^{SRO}$ (*Pnnm*) (b) oP20-$Li_{1/2}BC^{IB}$ and (c) $Li_{1/2}K_{1/6}BC$.

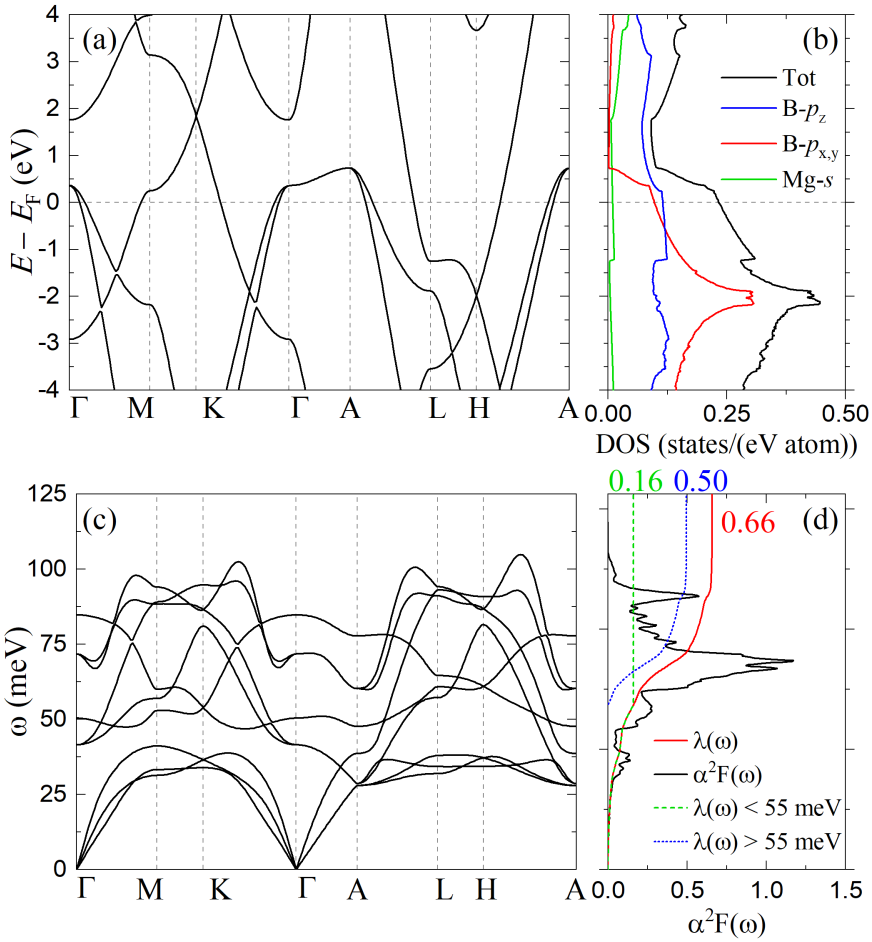

FIG. S23. Electronic and vibrational properties for MgB_2. Panel (a) shows the band structure and panel (b) the total and projected density of states. Panel (c) shows the phonon dispersion and panel (d) the Eliashberg spectral function $\alpha^2F(\omega)$ with total integrated e-ph coupling strength λ. The partial e-ph coupling strength from modes above and below 55 meV are shown as the dotted blue and dashed green lines, respectively.

TABLE S1. Structural and electronic information for select Li_xBC and Li_xM_yBC phases obtained with Quantum ESPRESSO [12]. The morphology of the Li_xBC phases is specified with superscript abbreviations defined in the main text. The AA or AA' c-axis stacking notation specifies whether the placement of B and C atoms in adjacent honeycomb layers follows the same (BB and CC) or alternating (BC and CB) sequences, respectively. The total DOS at the Fermi level (N) is listed along with partial DOS for BC-σ (N_σ) and BC-π (N_π) states. The level of hole or electron doping is given per BC formula unit. The full structural information for unit cells relaxed with VASP [13] is provided in CIF files.

Structure name	Space group	Pearson symbol	Lattice parameters (Å, °) a	b	c	β	Stacking sequence	Buckling (Å)	DOS [states/(eV atom)] N	N_σ	N_π	Doping level
$Li_{1/2}BC^{SRO}$	$Pnnm$	oP10	2.735	4.562	7.128		AA'	0.160	0.267	0.110	0.149	+1/2
$Li_{1/2}BC^{SRO}$	$Imm2$	oI10	2.728	7.083	4.601		AA	0.130	0.244	0.110	0.128	+1/2
$Li_{1/2}BC^{RH}$	$P\bar{3}m1$	hP5	2.718	—	6.420		AA'	0.032	0.240	0.116	0.117	+1/2
$Li_{1/2}BC^{SRO}$	$Pmma$	oP10	7.057	2.717	4.671		AA'	0.016	0.266	0.120	0.141	+1/2
$Li_{1/2}BC^{SRO}$	$P\bar{3}m1$	hP15	4.687	—	7.059		AA'	0.010	0.265	0.120	0.139	+1/2
$Li_{1/2}BC^{IB}$	$P2/m$	mP20	6.765	2.742	8.935	95.37	AA'		0.102	0.053	0.022	+1/2
	$Pmm2$	oP20	2.719	7.015	9.027		AA		0.113	0.047	0.061	+1/2
$Li_{1/2}BC^{BR}$	P/m	mP15	4.454	3.656	8.248	95.97	AA		0.083	0.083	0.000	+1/2
	P/m	mP30	8.241	3.650	9.004	94.89	AA		0.083	0.083	0.000	+1/2
$Li_{5/8}BC^{SRO}$	$C2/m$	mS42	5.412	5.412	7.088	91.22	AA'	0.026	0.240	0.109	0.122	+3/8
$Li_{2/3}BC^{SRO}$	$P6_3/mcm$	hP16	4.704	—	7.068		AA'	0.000	0.218	0.106	0.107	+1/3
$Li_{3/4}BC^{SRO}$	$Pmma$	oP22	5.455	4.710	7.068		AA'	0.000	0.211	0.099	0.107	+1/4
$Li_{5/6}BC^{SRO}$	$P\bar{3}1m$	hP17	4.730	—	7.054		AA'	0.009	0.235	0.097	0.130	+1/6
$Li_{7/8}BC^{SRO}$	$P\bar{3}m1$	hP23	5.470	—	7.040		AA'	0.003	0.239	0.090	0.141	+1/8
$Li_{1/2}Na_{1/4}BC$	$P2/m$	mP11	4.706	2.744	7.862	90.92	AA'	0.003	0.225	0.096	0.124	+1/4
$Li_{1/2}Na_{1/3}BC$	$P\bar{3}m1$	hP17	4.751	—	7.809		AA'	0.009	0.198	0.097	0.096	+1/6
$Li_{1/2}Na_{3/8}BC$	$P2/m$	mP23	7.846	2.759	9.489	90.43	AA'	0.023	0.214	0.093	0.114	+1/8
$Li_{1/2}Mg_{1/6}BC$	$P\bar{3}1m$	hP16	4.724	—	7.187		AA'	0.011	0.264	0.115	0.141	+1/6
$Li_{1/2}Ca_{1/6}BC$	$P\bar{3}m1$	hP16	4.722	—	7.850		AA'	0.009	0.199	0.099	0.093	+1/6
$Li_{1/2}K_{1/6}BC$	$P\bar{3}1m$	hP16	4.713	—	8.749		AA'	0.019	0.287	0.107	0.173	+1/3
$Li_{1/2}Ca_{1/3}BC$	$P\bar{3}m1$	hP17	4.818	—	7.651		AA'	0.000	0.153	0.003	0.098	−1/6
$Li_{1/2}Ca_{1/2}BC$	$P\bar{3}m1$	hP6	2.845	—	7.608		AA'	0.003	0.188	0.004	0.090	−1/2

TABLE S2. Settings used in the calculations of electronic, vibrational, and superconducting properties of Li_xBC and Li_xM_yBC phases performed with Quantum ESPRESSO (QE) [12] and EPW [14, 15].

Structure name	Space group	Pearson symbol	**k**-mesh (QE)	**q**-mesh (QE)	**k**-mesh (Wannier90)	# of Wannier Functions	Fine **k**-mesh (EPW)	Fine **q**-mesh (EPW)
$Li_{1/2}BC^{SRO}$	$Pnnm$	oP10	30×18×8	6×4×3	12×8×6	12	120×70×30	60×35×15
$Li_{1/2}BC^{SRO}$	$Imm2$	oI10	30×8×18	6×3×4	12×6×8	12	120×30×70	60×15×35
$Li_{1/2}BC^{RH}$	$P\bar{3}m1$	hP5	30×30×8	6×6×3	12×12×6	6	120×120×30	60×60×15
$Li_{1/2}BC^{SRO}$	$Pmma$	oP10	8×30×18	3×6×4	6×12×8	12	30×120×70	15×60×35
$Li_{1/2}BC^{SRO}$	$P\bar{3}m1$	hP15	18×18×8	5×5×3	10×10×6	18	70×70×30	35×35×15
$Li_{1/2}BC^{IB}$	$P2/m$	mP20	12×30×10	3×6×2	6×12×4	24	50×120×30	25×60×15
$Li_{1/2}BC^{IB}$	$Pmm2$	oP20	30×8×8	6×3×3	12×6×6	24	120×30×30	60×15×15
$Li_{1/2}BC^{BR}$	P/m	mP15	18×24×8	4×6×3	8×12×6	18	70×100×30	35×50×15
$Li_{1/2}BC^{BR}$	P/m	mP30	10×24×8	3×4×2				
$Li_{5/8}BC^{SRO}$	$C2/m$	mS42	18×18×8	4×4×3	8×8×6	24	70×70×30	35×35×15
$Li_{2/3}BC^{SRO}$	$P6_3/mcm$	hP16	18×18×8	4×4×3	8×8×6	18	70×70×30	35×35×15
$Li_{3/4}BC^{SRO}$	$Pmma$	oP22	18×18×8	4×4×3	8×8×6	24	70×70×30	35×35×15
$Li_{5/6}BC^{SRO}$	$P\bar{3}1m$	hP17	18×18×8	4×4×3	8×8×6	18	70×70×30	35×35×15
$Li_{1/2}Na_{1/4}BC$	$P2/m$	mP11	18×30×8	4×6×3	8×12×6	12	70×120×30	35×60×15
$Li_{1/2}Na_{1/3}BC$	$P\bar{3}m1$	hP17	18×18×8	4×4×3	8×8×6	18	70×70×30	35×35×15
$Li_{1/2}Na_{3/8}BC$	$P2/m$	mP23	10×30×8	3×4×2	6×8×4	24	30×120×30	15×60×15
$Li_{1/2}K_{1/6}BC$	$P\bar{3}1m$	hP16	18×18×8	5×5×3	10×10×6	18	70×70×30	35×35×15
$Li_{1/2}Mg_{1/6}BC$	$P\bar{3}1m$	hP16	18×18×8	5×5×3	10×10×6	18	70×70×30	35×35×15
$Li_{1/2}Ca_{1/6}BC$	$P\bar{3}m1$	hP16	18×18×8	4×4×3	8×8×6	18	70×70×30	35×35×15
$Li_{1/2}Ca_{1/3}BC$	$P\bar{3}m1$	hP17	18×18×8	4×4×3	8×8×6	18	70×70×30	35×35×15
$Li_{1/2}Ca_{1/2}BC$	$P\bar{3}m1$	hP6	30×30×8	6×6×3	12×12×6	6	120×120×30	60×60×15

[1] B. Kalkan and E. Ozdas, ACS Appl. Mater. Interfaces **11**, 4111 (2019).
[2] A. M. Fogg, P. R. Chalker, J. B. Claridge, G. R. Darling, and M. J. Rosseinsky, Phys. Rev. B **67**, 245106 (2003).
[3] L. Zhao, P. Klavins, and K. Liu, J. Appl. Phys. **93**, 8653 (2003).
[4] R. D. Shannon, Acta Cryst. A **32**, 751 (1976).
[5] A. Jain, S. P. Ong, G. Hautier, W. Chen, W. D. Richards, S. Dacek, S. Cholia, D. Gunter, D. Skinner, G. Ceder, and K. A. Persson, APL Materials **1**, 011002 (2013).
[6] S. Kharabadze, M. Meyers, C. R. Tomassetti, E. R. Margine, I. I. Mazin, and A. N. Kolmogorov, Phys. Chem. Chem. Phys. **25**, 7344 (2023).
[7] N. Emery, C. Hérold, M. d'Astuto, V. Garcia, C. Bellin, J. F. Marêché, P. Lagrange, and G. Loupias, Phys. Rev. Lett. **95**, 087003 (2005).
[8] S. Delacroix, F. Igoa, Y. Song, Y. L. Godec, C. Coelho-Diogo, C. Gervais, G. Rousse, and D. Portehault, Inorg. Chem. **60**, 4252 (2021).
[9] R. Miao, G. Huang, and J. Yang, Solid State Commun. **233**, 30 (2016).
[10] J. Klimeš, D. R. Bowler, and A. Michaelides, J. Phys. Condens. Matter **22**, 022201 (2010).
[11] J. Klimeš, D. R. Bowler, and A. Michaelides, Phys. Rev. B **83**, 195131 (2011).
[12] P. Giannozzi, O. Andreussi, T. Brumme, O. Bunau, M. B. Nardelli, M. Calandra, R. Car, C. Cavazzoni, D. Ceresoli, M. Cococcioni, N. Colonna, I. Carnimeo, A. D. Corso, S. de Gironcoli, P. Delugas, R. A. DiStasio, A. Ferretti, A. Floris, G. Fratesi, G. Fugallo, R. Gebauer, U. Gerstmann, F. Giustino, T. Gorni, J. Jia, M. Kawamura, H.-Y. Ko, A. Kokalj, E. Küçükbenli, M. Lazzeri, M. Marsili, N. Marzari, F. Mauri, N. L. Nguyen, H.-V. Nguyen, A. O. de-la Roza, L. Paulatto, S. Poncé, D. Rocca, R. Sabatini, B. Santra, M. Schlipf, A. P. Seitsonen, A. Smogunov, I. Timrov, T. Thonhauser, P. Umari, N. Vast, X. Wu, and S. Baroni, J. Phys. Condens. Matter **29**, 465901 (2017).
[13] G. Kresse and J. Furthmüller, Phys. Rev. B **54**, 11169 (1996).
[14] S. Poncé, E. R. Margine, C. Verdi, and F. Giustino, Comput. Phys. Commun. **209**, 116 (2016).
[15] H. Lee, S. Poncé, K. Bushick, S. Hajinazar, J. Lafuente-Bartolome, J. Leveillee, C. Lian, J.-M. Lihm, F. Macheda, H. Mori, H. Paudyal, W. H. Sio, S. Tiwar, M. Zacharias, X. Zhang, N. Bonini, E. Kioupakis, E. R. Margine, and F. Giustino, npj Comput. Mater. **9**, 156 (2023).